NANO LETTERS
Cite This: Nano Lett. XXXX, XXX, XXX−XXX
Letter
pubs.acs.org/NanoLett

Ultrasonic Nebulization for TEM Sample Preparation on Single-Layer Graphene Grids

Joshua G. Hinman,[†,§] Jordan J. Hinman,[†,§] Blanka E. Janicek,[‡] Pinshane Y. Huang,[‡] Kenneth S. Suslick,[†] and Catherine J. Murphy*[,†]

[†]Department of Chemistry, University of Illinois at Urbana−Champaign, 600 S. Mathews Avenue, Urbana, Illinois 61801, United States

[‡]Department of Materials Science and Engineering, University of Illinois at Urbana−Champaign, 1304 W. Green Street, Urbana, Illinois 61801, United States

Supporting Information

ABSTRACT: Spray-coating using ultrasonic nebulization is reported for depositing nanoparticles on a TEM grid without many of the drying artifacts that are often associated with drop-casting. Spray-coating is suitable for preparing TEM samples on fragile support materials, such as suspended single-layer graphene, that rupture when samples are prepared by drop-casting. Additionally, because ultrasonic nebulization produces uniform droplets, nanoparticles deposited by spray-coating occur on the TEM grid in clusters, whose size is dependent on the concentration of the nanoparticle dispersion, which may allow the concentration of nanoparticle dispersions to be estimated using TEM.

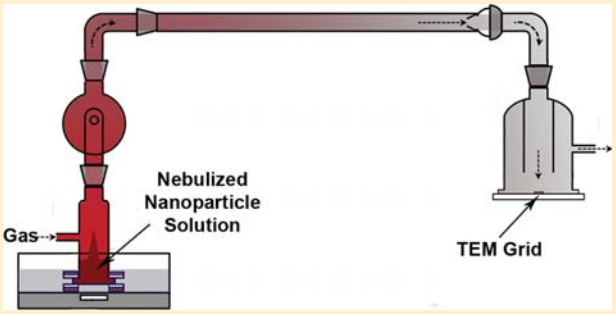

KEYWORDS: *Nanoparticle, nebulization, graphene, transmission electron microscopy, spray*

Transmission electron microscopy (TEM) is one of the most powerful and versatile tools for the analysis and characterization of nanomaterials. Although TEM is most often used to study hard, inorganic nanomaterials, techniques such as staining[1] and cryo-TEM[2,3] also allow researchers to glean insights about ligands and soft coatings on nanoparticles. Advances in the resolution and sensitivity of analytical scanning transmission electron microscopy (STEM) methods such as energy dispersive spectroscopy (STEM-EDS)[4] and electron energy loss spectroscopy (STEM-EELS)[5] have made it possible to obtain spatially resolved information about the chemical composition of nanomaterials and their surfaces.[6] Meanwhile, aberration-corrected TEM/STEM imaging and electron tomography have enabled detailed measurements of nanoparticles surface structure, including their facet termination and surface strains.[7]

In contrast to the increasingly complex measurements available using analytical electron microscopy, TEM sample preparation methods for colloidal nanoparticles have remained surprisingly unsophisticated. Most commonly, dispersions of nanoparticles are drop-cast onto a thin film and the solvent is allowed to evaporate.[8,9] While drop-casting is perfectly suitable for many samples, it often introduces drying artifacts, with the nanoparticles tending to form aggregates, especially at the edge of the drying drop leading to "coffee-ring" effects,[8,10−12] potentially leading to bias in the analysis of nanoparticles as depletion forces cause similar nanoparticles to be found close to one another.[13,14] Furthermore, drop-casting is not suitable for every type of support film, especially fragile support membranes such as suspended single-layer graphene, which can provide an ultralow background support for direct images of ligand coatings.[15,16]

Here we describe a technique for TEM sample preparation that utilizes ultrasonic nebulization to spray-coat nanoparticles onto a TEM grid and is suitable for depositing nanoparticles even on fragile support membranes such as single-layer graphene. Ultrasonic spray-coating has been widely used to deposit particle and polymer coatings on many different surfaces.[17−24] While a colloidal dispersion can be nebulized in a variety of ways, ultrasonic nebulization is a convenient method.[25−28] In an ultrasonic nebulizer, a transducer generates an ultrasonic frequency in a liquid. At sufficiently high power, droplets are ejected from capillary waves on the surface of the liquid, generating a mist.[29] For colloidal nanoparticles, if the nanoparticle concentration is low enough, then there are only a few nanoparticles per droplet when the nanoparticles are deposited as an ultrafine (micron-sized) mist, which avoids the drying artifacts associated with drop-casting.

In this study, we demonstrate that spray-coating can be used to prepare TEM samples of aqueous nanoparticles on large-area, suspended single-layer graphene without damage to the

Received: December 22, 2018
Revised: February 3, 2019
Published: February 11, 2019

DOI: 10.1021/acs.nanolett.8b05117
Nano Lett. XXXX, XXX, XXX−XXX

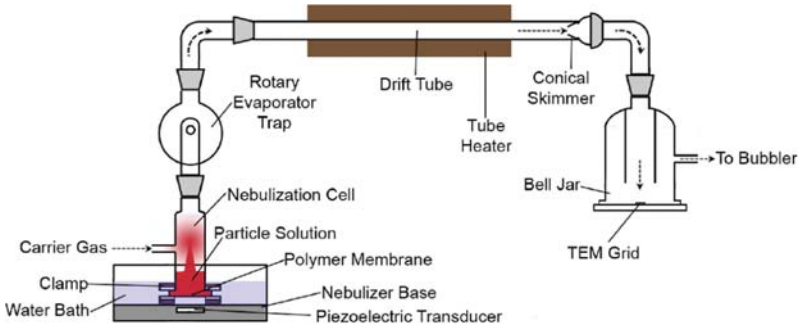

Figure 1. A schematic diagram of the ultrasonic spray-coating apparatus. A piezoelectric transducer is used to nebulize a solution of nanoparticles. The nebulized mist is propelled by a carrier gas through a bump trap to a drift tube. After passing through a skimmer, the remaining droplets travel into a bell jar where they deposit on a TEM grid. Any remaining aerosol is trapped by a bubbler.

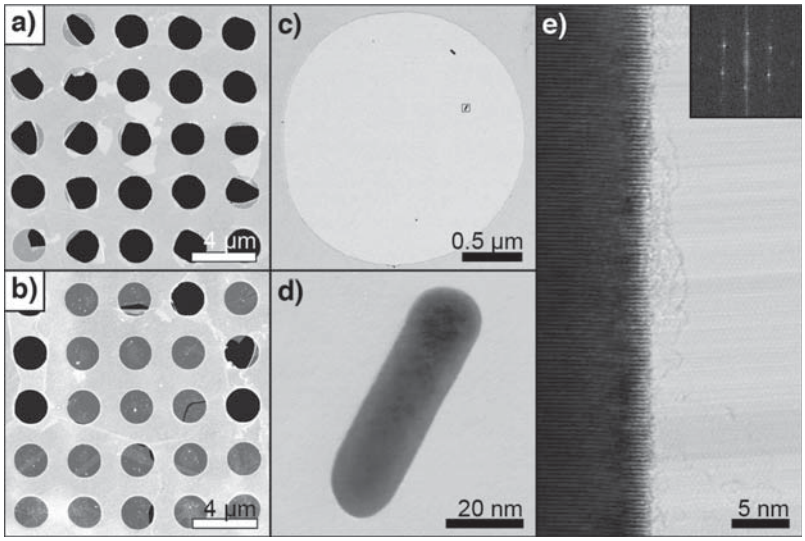

Figure 2. Electron microscopy images of nanoparticles deposited on suspended single-layer graphene. Typical low-magnification scanning electron microscope images showing (a) ruptured suspended graphene on a TEM grid after drop-casting water (the black color indicating that the graphene is lost and a gaping hole remains) and (b) intact suspended graphene (appearing gray) on a TEM grid after spray-depositing aqueous nanoparticles. Note that as a result of our transfer techniques we observe 60−70% intact, nonruptured graphene coverage both prior to and after spray nebulization. (c−e) Bright-field STEM images of ligand-coated gold nanorods after spray deposition onto graphene. (c) A typical distribution of spray-deposited nanoparticles on suspended graphene over a single hole in the TEM grid. In order to maximize the deposition of isolated particles, a low nanoparticle concentration of 1 nM was used. (d) A higher magnification image of the particle indicated by the red box in part c. (e) Aberration-corrected bright-field STEM image (fast Fourier transform of the graphene support in the inset) of the edge of the AuNR shows lattice fringes from the gold and graphene, as well as contrast from the organics on the surface of the gold particle made visible via the graphene substrate.

graphene membrane. In addition, while it is conventionally not possible to measure nanoparticle concentration using TEM,[30] it is possible to estimate nanoparticle concentration using simple particle counting techniques from spray-coated samples, because the droplets generated using ultrasound are reasonably uniform in size.

We adopted an ultrasonic spray-coating technique using an apparatus depicted in Figure 1. We use a home-built setup using a commercial ultrasonic nebulizer, similar to what is in a humidifier, that provides a maximum power of 12.5 W (see the Supporting Information for details). Colloidal nanoparticles were injected into a glass cell over an ultrasonic transducer that was used to generate a fine mist. A polymer membrane on the bottom of the cell separated the nanoparticle dispersion from the water bath below while allowing the conduction of the ultrasound into the cell. In addition to the capillary waves, ultrasonic irradiation also induces macroscopic disturbances in the nanoparticle solution, which may produce large droplets. Additionally, droplets may collide and coalesce in the thick mist that is produced. To filter larger droplets and splashes, a bump trap was placed over the nebulization cell. A carrier gas was used to convey the nebulized nanoparticle solution through the bump trap into a horizontal drift tube. At the end of the drift tube, a conical skimmer, made from a vacuum funnel gasket with a 1 cm diameter opening, was added to filter out any large particles that may have formed via droplet coalescence through the drift tube.

The remaining droplets then flowed down to deposit on a TEM grid that was placed on a clean piece of silicon or a glass slide. The carrier gas and any remaining suspended particles flowed through a bubbler to collect the nanoparticles and prevent their release into the air. Additional procedural and synthetic details can be found in the Supporting Information. Note that inhalation of nanoparticles represents a potential health hazard; ultrasonic spray-coating for the deposition of nanomaterials should always be carried out in a fume hood to minimize the risk of inhalation.

DOI: 10.1021/acs.nanolett.8b05117
Nano Lett. XXXX, XXX, XXX−XXX

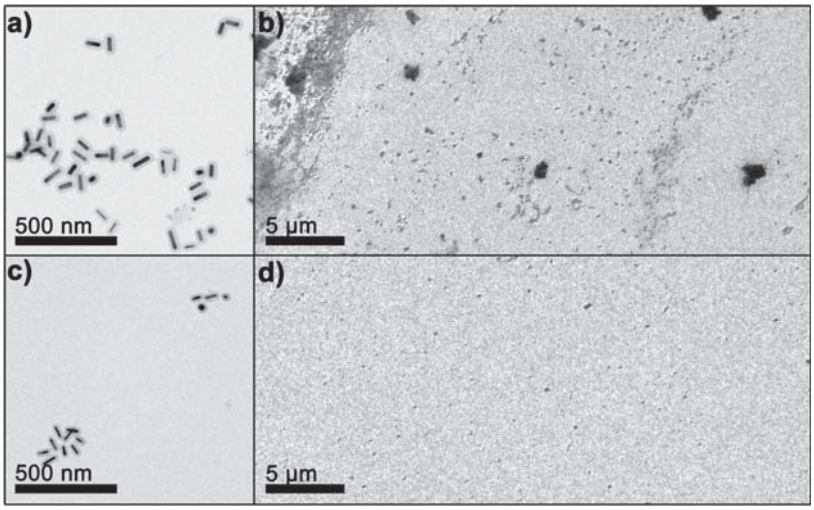

Figure 3. (a, b) Typical low-magnification TEM images of drop-cast silica-coated AuNRs on an amorphous carbon-coated TEM grid. (c, d) Typical low-magnification TEM images of spray-deposited silica-coated AuNRs show two clusters of spray-deposited nanorods. While drop-cast AuNRs aggregate as they dry, spray-coated AuNRs are evenly deposited on the TEM sample in uniformly sized clusters.

Ultrasonic nebulization allows for sample preparation on fragile support materials such as suspended single-layer graphene. Single-layer graphene offers unrivaled high-resolution TEM and STEM imaging of low atomic number nanomaterials and has even allowed for the imaging of organic ligands on nanoparticles.[15,16] Preparing TEM samples on single-layer graphene is challenging because drop-casting colloidal nanoparticles (especially aqueous nanoparticles) onto graphene can cause ruptures, similar to what has been previously reported for drop-casting water on graphene to measure contact angles.[31] Current methods to prepare samples of nanoparticles on graphene involve drop-casting the nanoparticles and nanoscale graphene flakes onto TEM grids with a lacey carbon support.[31] These methods produce limited areas of single-layer graphene suitable for high-resolution imaging because large fractions of the graphene flakes are typically folded or are overlapping other graphene flakes or the lacey carbon support. We tested the utility of our nebulization methods for depositing gold nanorods (AuNRs) on graphene-coated TEM grids. First, we prepared graphene-coated TEM grids by transferring a millimeter-scale sheet of graphene grown by chemical vapor deposition to a TEM grid containing an array of 2 μm holes, as described in the Supporting Information. These methods produce TEM supports where 60−70% of the holes are covered by suspended single-layer graphene. These areas of suspended graphene represent the usable area for TEM imaging. Roughly 85% of these graphene regions ruptured after water was drop-cast and dried (Figure 2a). In contrast, we do not observe membrane rupture following ultrasonic spray-coating of nanoparticles on suspended graphene (Figure 2b). Figure 2c shows a wide-field view of a single-layer graphene grid, onto which nanoparticles have been deposited; only a few nanoparticles/clusters are evident from this dilute solution. A red box outlines one such cluster, and a magnified image of a ligand-coated gold nanorod in this red box is shown in Figure 2d. Figure 2e shows an aberration-corrected bright-field STEM image of the surface of a gold nanorod and corresponding fast Fourier transform showing lattice fringes from the graphene support. We also observe contrast from surface organics on the particle, which are visible against the low background of the atomically thin graphene substrate.

We compared the coverage of silica-coated gold nanorods in ethanol deposited on TEM grids that had been ultrasonically spray-coated with those that had been prepared by drop-casting. TEM images of typical nanoparticle distributions for drop-cast 0.1 nM silica-coated AuNRs and spray-coated 0.1 nM silica-coated AuNRs are shown in Figure 3. Drop-casting results in irregular coverage on the TEM grid (Figure 3a,b). Some regions in the sample have sparse coverage, while in other areas the AuNRs are densely packed together. Aggregates of nanoparticles, likely formed during the drying process, are also apparent. In comparison, spray-coating (Figure 3c,d) results in a random distribution of small clusters of nanoparticles. The density of coverage can be tuned by increasing or decreasing the time for spray-coating. (We note that continuous spray-coating for too long can wet the TEM grid, which may lead to drying effects; it is better to increase the spray-coating time by implementing a series of short periods of spray-coating followed by periods during which only the carrier gas is flowing.) Reducing the number of nanoparticles that occur in each cluster can be accomplished simply by diluting the nanoparticles injected into the nebulization cell. For dilute enough nanoparticle solutions, a majority of the nanoparticles will be deposited alone.

On TEM grids prepared using our spray-coating method, the number of nanoparticles in any given cluster is similar throughout the sample. This is due to the fact that the droplets resulting from ultrasonic nebulization of a liquid have a uniform, well-defined size. The number median diameter of the droplets (D) is proportional to the size of the surface capillary waves, dependent on the surface tension (γ) and density (ρ) of the liquid, as well as the frequency (F) of the ultrasound, as described in Lang's equation:[32]

$$D = 0.34(8\pi\gamma/(\rho F^2))^{1/3} \quad (1)$$

For example, pure ethanol irradiated at 1.65 MHz has a number median droplet diameter of about 2 μm. As the solvent in each droplet evaporates, either as it passes through the drift tube or after it is deposited on the TEM grid, the nanoparticles are drawn together in clusters. The uniformity in droplet size

DOI: 10.1021/acs.nanolett.8b05117
Nano Lett. XXXX, XXX, XXX−XXX

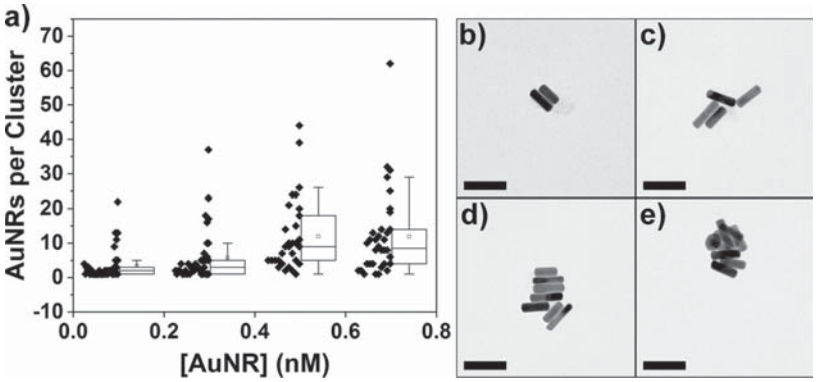

Figure 4. (a) Box and whisker plots of the number of AuNRs per cluster for samples prepared from different concentrations of AuNRs. TEM images of typical clusters prepared from 0.1, 0.3, 0.5, and 0.7 nM AuNRs are shown in parts b–e, respectively. Scale bars are 100 nm.

allows the number of particles per droplet, and therefore the number of nanoparticles per cluster on the TEM grid, to be controlled by changing the particle concentration, or by analyzing the number of particles in each cluster, it is also possible to estimate the concentration of the ultrasonically nebulized nanoparticle solution.

Measuring nanoparticle concentration is not often very straightforward. For intensely colored AuNRs, the preferred method involves comparing the UV–vis extinction of the longitudinal localized surface plasmon resonance (LSPR) to the gold concentration determined by inductively coupled plasma optical emission spectrometry (ICP-OES) or ICP mass spectrometry (ICP-MS) and the dimensions of the AuNRs as determined by TEM to find an extinction coefficient.[33,34] For nanoparticles that lack a spectroscopic handle, dilute colloidal suspensions rely on numerous (possibly destructive) steps. However, for colloidally stable dispersions of nanoparticles, the median number density of nanoparticles per ultrasonically nebulized droplet should reflect the concentration of nanoparticles in the dispersion, providing a general means of estimating nanoparticle concentration independent of nanoparticle composition. As TEM is regularly used to measure nanoparticle dimensions, a deposition method that can also supply an estimate of nanoparticle concentration adds value.

To demonstrate that it is possible to estimate nanoparticle concentration independent of nanoparticle composition, we used ultrasonic spray-coating to prepare TEM samples from 0.1, 0.3, 0.5, and 0.7 nM 11-mercaptoundecanoic acid (MUA)-capped AuNR solutions in 5 mM NH_4OH (for colloidal stability). The AuNRs were measured to have average dimensions of 70 ± 14 by 21 ± 2 nm, and their concentration was spectroscopically determined using an extinction coefficient of 1.6×10^{10} M^{-1} cm^{-1}.[33] TEM images were taken of at least 30 clusters for each concentration, and the number of nanorods was then counted for each cluster. AuNRs that were in contact with one another were considered to be in the same cluster. For aqueous samples, heating the drift tube to 150 °C ensured that solvent evaporated prior to the deposition of the clusters on the TEM grid to make it easier to distinguish one cluster from another. Ultimately, the conical skimmer at the end is optional; clusters have similarly sized geometric standard deviations independent of the skimmer presence.

Figure 4a shows box and whisker plots alongside the data for the number of AuNRs deposited per cluster for the different concentrations of AuNRs. Typical clusters for each concentration are shown in Figure 4b–e. Since the size of droplets produced by ultrasonic nebulization more or less follows a log-normal distribution,[35,36] it is not surprising that the cluster sizes are also log-normal distributed. The median cluster size was estimated by finding the geometric mean (GM) for the cluster of each concentration of AuNRs. The concentration was calculated from the GM cluster size, x, using eq 2

$$[\text{AuNR}] = x/(N_A V_{\text{droplet}}) \quad (2)$$

where N_A is Avogadro's number and V_{droplet} corresponds to the volume of a droplet with diameter D as described by eq 1, assuming γ and ρ for pure water or 72 mN/m and 1000 kg/m^3, respectively. These concentrations are plotted in Figure 5a against the concentrations of the AuNR solutions determined via their UV–vis extinction. Error bars show the geometric standard deviation calculated from the spread in cluster sizes; as expected for log-normal distributions, the spread in cluster sizes increases for larger clusters. This does not represent an increase in uncertainty in measuring the concentration at these sizes. In Figure S2, similar results are plotted for cetyltrimethylammonium bromide (CTAB)-capped AuNRs. The concentrations estimated from counting the AuNRs in the clusters of CTAB-capped AuNRs are within 1.4–1.5 times the UV–vis concentration.

Clearly, using the number of nanoparticles per cluster is a relatively crude measure of nanoparticle concentration. The concentrations estimated from the clusters of MUA-capped AuNRs are 1.2–2.5 times the UV–vis concentration. The greatest disagreement was found for the 0.1 nM sample. By rearranging eq 2 and solving for x, it can be shown that a cluster size of 0.8 would be expected for nanoparticles with a concentration of 0.1 nM, meaning less than 1 particle per droplet. Therefore, at very low concentrations, this method gives an overestimation of the concentration. At the other end of the range, this technique is limited by the ability to reliably count the number of nanorods in each cluster. As clusters become too large and nanoparticles are stacked on top of one another, it can become difficult to distinguish between them in TEM images. Long nebulization periods lead to different particle concentrations due to evaporation; therefore, the longest deposition times used were 10 min.

Nanoparticle surface chemistry may also affect the accuracy of cluster sizing for estimating nanoparticle concentration. TEM samples of silica-coated AuNRs in ethanol were also prepared using ultrasonic spray-coating. Estimates of the concentration for different concentrations of silica-coated AuNRs were 5.6–6.9 times greater than the concentrations

DOI: 10.1021/acs.nanolett.8b05117
Nano Lett. XXXX, XXX, XXX–XXX

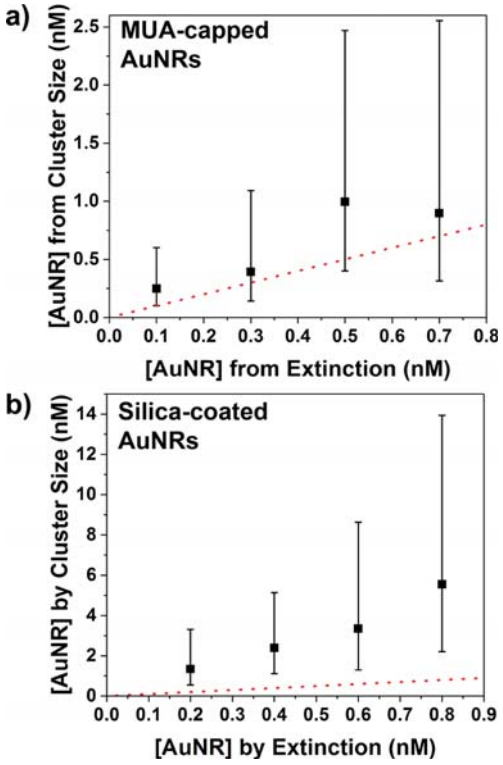

Figure 5. Concentration of (a) MUA-capped AuNRs and (b) silica-coated AuNRS in ethanol. Concentrations on the *y*-axis were estimated from the geometric mean of the size of the clusters that were deposited via ultrasonic spray-coating, while concentrations on the *x*-axis were measured by UV−vis extinction spectrophotometry. The dotted red line, added as a guide to the eye, shows the relationship of the two methods were in perfect agreement. Error bars depict the geometric standard deviation, which increases as the mean of the log-normal distribution increases. The nanomaterials in part b were not as colloidally stable as those in part a, leading to a worse agreement with the theoretically predicted concentrations.

as determined by UV−vis (Figure 5b). While the MUA-capped AuNRs, which had a ζ-potential of -43.5 ± 1.3 mV, were colloidally stable, the silica-coated AuNRs, with a ζ-potential of -12.8 ± 1.5 mV, would settle over the course of several hours. We therefore suggest that nanoparticle concentration estimates using this approach are best-suited for colloidally stable materials.[37] While coalescence of nebulized droplets could also lead to greater cluster sizes, and apparent concentration, it does not have a significant effect on our results (see Supporting Information). To demonstrate that spray nebulization can estimate the nanomaterial concentration independent of nanoparticle size and morphology, we used ultrasonic spray-coating to prepare a TEM sample from 4.0 nM citrate-capped gold nanoparticles (AuNPs) (see Figure S3). The concentration estimated from the geometric mean size of the clusters was 2.7 nM, within a factor of 2 compared to the concentration as determined by UV−vis.

We have demonstrated that ultrasonic spray-coating can be used as an alternative to drop-casting for preparing TEM samples from nanoparticle dispersions. While it is difficult to prevent drying artifacts such as aggregation and the formation of coffee rings when preparing samples by drop-casting, spray-coating results in an even distribution of nanoparticles. For fragile TEM support films like suspended single-layer graphene, spray-coating enables TEM samples that would otherwise be impossible to prepare via drop-casting due to a rupture of the support film. Because ultrasonic nebulization produces droplets of uniform size, spray-coating results in the deposition of clusters of nanoparticles. We have shown that the number of nanoparticles per cluster varies linearly with nanoparticle concentration for colloidally stable systems, which can be leveraged to estimate nanoparticle concentration.

■ ASSOCIATED CONTENT

Supporting Information

The Supporting Information is available free of charge on the ACS Publications website at DOI: 10.1021/acs.nanolett.8b05117.

AuNR synthesis, silica coating of AuNRs, MUA functionalization of AuNRs, ultrasonic nebulization for TEM sample preparation, instrumentation, graphene transfer method, estimation of nebulized droplet size distribution, and estimation of CTAB-capped AuNR concentration from cluster sizes (PDF)

■ AUTHOR INFORMATION

Corresponding Author

*E-mail: murphycj@illinois.edu.

ORCID

Joshua G. Hinman: 0000-0002-1744-6661
Kenneth S. Suslick: 0000-0001-5422-0701
Catherine J. Murphy: 0000-0001-7066-5575

Author Contributions

[§]J.G.H. and J.J.H. contributed equally.

Notes

The authors declare no competing financial interest.

■ ACKNOWLEDGMENTS

This work was supported by the National Science Foundation (CHE-1608743 and the Illinois MRSEC, DMR-1720633) and by the Packard Foundation Fellowship. Portions of this work were carried out at the Materials Research Laboratory Central Research Facilities, University of Illinois at Urbana−Champaign. Portions of this work made use of the Cornell Center for Materials Research Shared Facilities, which are supported through the NSF MRSEC program (DMR-1719875).

■ REFERENCES

(1) Yang, J. A.; Murphy, C. J. *Langmuir* **2012**, *28*, 5404−5416.
(2) Burrows, N. D.; Penn, R. L. *Microsc. Microanal.* **2013**, *19*, 1542−1553.
(3) Wang, Y.; Zeiri, O.; Neyman, A.; Stellacci, F.; Weinstock, I. A. *ACS Nano* **2012**, *6*, 629−640.
(4) Jackson, S. R.; McBride, J. R.; Rosenthal, S. J.; Wright, D. W. *J. Am. Chem. Soc.* **2014**, *136*, 5261−5263.
(5) Kim, J.-Y.; Han, M.-G.; Lien, M.-B.; Magonov, S.; Zhu, Y.; George, H.; Norris, T. B.; Kotov, N. A. *Sci. Adv.* **2018**, *4*, No. e1700682.
(6) Chaudhuri, R. G.; Paria, S. *Chem. Rev.* **2012**, *112*, 2373−2433.
(7) Goris, B.; Bals, S.; van den Broek, W.; Carbo-Argibay, E.; Gomez-Grana, S.; Liz-Marzan, L. M.; van Tendeloo, G. *Nat. Mater.* **2012**, *11*, 930−935.
(8) Michen, B.; Geers, C.; Vanhecke, D.; Endes, C.; Rothen-Rutishauser, B.; Balog, S.; Petri-Fink, A. *Sci. Rep.* **2015**, *5*, 9793.
(9) Williams, D. B.; Carter, C. B. *The Transmission Electron Microscope: A Textbook for Materials Science*; Springer: Boston, 1996.

DOI: 10.1021/acs.nanolett.8b05117
Nano Lett. XXXX, XXX, XXX−XXX

(10) Dieckmann, Y.; Cölfen, H.; Hofmann, H.; Petri-Fink, A. *Anal. Chem.* **2009**, *81*, 3889−3895.
(11) Domingos, R. F.; Baalousha, M. A.; Ju-Nam, Y.; Reid, M. M.; Tufenkji, N.; Lead, J. R.; Leppard, G. G.; Wilkinson, K. *Environ. Sci. Technol.* **2009**, *43*, 7277−7284.
(12) Majumder, M.; Rendall, C. S.; Eukel, J. A.; Wang, J. Y. L.; Behabtu, N.; Pint, C. L.; Liu, T.-Y.; Orbaek, A. W.; Mirri, F.; Nam, J.; Barron, A. R.; Hauge, R. H.; Schmidt, H. K.; Pasquali, M. *J. Phys. Chem. B* **2012**, *116*, 6536−6542.
(13) Haw, M. D.; Gillie, M.; Poon, W. C. K. *Langmuir* **2002**, *18*, 1626−1633.
(14) Park, K.; Koerner, H.; Vaia, R. A. *Nano Lett.* **2010**, *10*, 1433−1439.
(15) Panthani, M. G.; Hessel, C. M.; Reid, D.; Casillas, G.; José-Yacamán, M.; Korgel, B. A. *J. Phys. Chem. C* **2012**, *116* (42), 22463−22468.
(16) Lee, Z.; Jeon, K.-J.; Dato, A.; Erni, R.; Richardson, T. J.; Frenklach, M.; Radmilovic, V. *Nano Lett.* **2009**, *9* (9), 3365−3369.
(17) van den Ham, E. J.; Elen, K.; Bonneux, G.; Maino, G.; Notten, P. H. L.; Van Bael, M. K.; Hardy, A. *J. Power Sources* **2017**, *348*, 130−137.
(18) van den Ham, E. J.; Elen, K.; Kokal, I.; Yağci, B.; Peys, N.; Bonneux, G.; Ulu, F.; Marchal, W.; Van Bael, M. K.; Hardy, A. *RSC Adv.* **2016**, *6*, 51747−51756.
(19) van den Ham, E. J.; Gielis, S.; Van Bael, M. K.; Hardy, A. *ACS Energy Lett.* **2016**, *1*, 1184−1188.
(20) Jang, H. D.; Chang, H.; Cho, K.; Kim, F.; Sohn, K.; Huang, J. *Aerosol Sci. Technol.* **2010**, *44*, 1140−1145.
(21) Liu, S.; Zhang, X.; Yin, M.; Feng, H.; Zhang, J.; Zhang, L.; Xie, W. *ACS Appl. Energy Mater.* **2018**, *1*, 103−112.
(22) Liu, H.-S.; Chang, W.-C.; Chou, C.-Y.; Pan, B.-C.; Chou, Y.-S.; Liou, G.-S.; Liu, C.-L. *Sci. Rep.* **2017**, *7*, 1−10.
(23) Liu, S.; Zhang, X.; Wang, S.; Feng, H.; Zhang, J.; Yang, H.; Zhang, L.; Xie, W. *Org. Electron.* **2018**, *52*, 264−271.
(24) Dominguez, M. A.; Luna-Lopez, J. A.; Ceron, S. *Thin Solid Films* **2018**, *645*, 278−281.
(25) Mahurin, S. M.; Cheng, M.-D. *Nanotoxicology* **2007**, *1*, 130−138.
(26) Cho, Y.-S.; Yi, G.-R.; Chung, Y. S.; Park, S. B.; Yang, S.-M. *Langmuir* **2007**, *23*, 12079−12085.
(27) Park, J. Y.; McMurry, P. H.; Park, K. *Aerosol Sci. Technol.* **2012**, *46*, 354−360.
(28) Jeon, S.; Oberreit, D. R.; Van Schooneveld, G.; Hogan, C. J. *Analyst* **2016**, *141*, 1363−1375.
(29) Deepu, P.; Peng, C.; Moghaddam, S. *Exp. Therm. Fluid Sci.* **2018**, *92*, 243−247.
(30) Bell, N. C.; Minelli, C.; Tompkins, J.; Stevens, M. M.; Shard, A. G. *Langmuir* **2012**, *28*, 10860−10872.
(31) Belyaeva, L. A.; van Deursen, P. M. G.; Barbetsea, K. I.; Schneider, G. F. *Adv. Mater.* **2018**, *30*, 1703274.
(32) Lang, R. J. *J. Acoust. Soc. Am.* **1962**, *34*, 6−8.
(33) Orendorff, C. J.; Murphy, C. J. *J. Phys. Chem. B* **2006**, *110*, 3990−3994.
(34) Chang, H.-H.; Murphy, C. *Chem. Mater.* **2018**, *30*, 1427−1435.
(35) Rodes, C.; Smith, T.; Crouse, R.; Ramachandran, G. *Aerosol Sci. Technol.* **1990**, *13*, 220−229.
(36) Davidson, W. J.; Dennis, J.; The, S.; Litoski, B.; Pieron, C.; Leigh, R. *Can. Respir. J.* **2014**, *21* (2), 101−106.
(37) Farinas, J. C.; Moreno, R.; Mermet, J.-M. *J. Anal. At. Spectrom.* **1994**, *9*, 841−849.

DOI: 10.1021/acs.nanolett.8b05117
Nano Lett. XXXX, XXX, XXX−XXX